Chapter 6

Quasielastic Light Scattering Study of Amyloid β-Protein Fibrillogenesis

Aleksey Lomakin and David B. Teplow

Abstract

Quasielastic light scattering (QLS) spectroscopy is a noninvasive optical method for studying the dynamic properties of macromolecular solutions. Its most important application is the determination of diffusion coefficients, from which the sizes of particles in solution may be estimated. The technique thus is particularly useful for monitoring assembly (polymerization and aggregation) reactions without the need for removing aliquots from the assembly system or disrupting the assembly process in any other way. We discuss here two of the most important aspects of QLS: (1) measurement of the correlation function of the scattered light intensity and (2) the use of this correlation function to reconstruct the distribution of sizes of the scattering particles. The ability to monitor the temporal evolution of particle size provides a powerful tool for studying protein assembly. We illustrate here how QLS has been applied to elucidate features of the oligomerization and fibrillogenesis of the amyloid β-protein, Aβ, thought to be the causative agent of Alzheimer's disease.

Key words: Dynamic light scattering, Hydrodynamic radius, Aggregation, Fibrillogenesis, Amyloid, Alzheimer's disease

1. Introduction

Quasielastic light scattering (QLS), also known as dynamic light scattering (DLS), is an optical method for the determination of diffusion coefficients of particles in solution (1–3). The QLS method is rapid, sensitive, noninvasive, and quantitative. QLS measures the fluctuations in intensity of light scattered from a sample irradiated by a laser. These fluctuations contain information about the motion of the scattering particles, thus allowing determination of diffusion coefficients of the particles in the sample solution. The diffusion coefficients depend on particle size and shape and also are affected by inter-particle interactions. The ability to monitor the temporal evolution of these parameters makes

Einar M. Sigurdsson et al. (eds.), *Amyloid Proteins: Methods and Protocols*, Methods in Molecular Biology, vol. 849,
DOI 10.1007/978-1-61779-551-0_6,

QLS a useful tool for studying particle aggregation and, in particular, for monitoring protein assembly.

We discuss here the application of QLS to the study of protein assembly. Abnormal protein assembly is associated with a number of neurodegenerative diseases, including Alzheimer's, Huntington's, Parkinson's, and prion diseases (for a review, see (4)), as well as a variety of systemic amyloidoses (5). In each case, proteins that exist normally in a soluble, unaggregated state form oligomers and fibrils that cause cell and tissue injury, generally leading to death. QLS can monitor protein aggregation with high sensitivity and resolution (6), allowing determination of fundamental parameters of protein self-assembly, including rates of fibril nucleation and elongation, number of monomers in a fibril, fibril length, and activation energy for monomer addition. Importantly, the ability to determine these parameters enables structure-activity studies that suggest physical mechanisms responsible for sporadic and familial (mutation-induced) forms of AD (7) and other amyloidosis. This knowledge is critical for the conception and execution of knowledge-based therapeutic strategies.

2. General Principles of QLS

At a point of observation, the scattered electromagnetic field is a sum of electromagnetic waves scattered by all particles illuminated by the incident wave:

$$\mathbf{E} = \sum_k \mathbf{E}_k \exp(-i\omega t + i\mathbf{q}\cdot\mathbf{r}_k), \tag{1}$$

where E_k is the amplitude of the scattered wave produced by the kth particle located at position $\mathbf{r}_k$, and ω is the frequency of light, $\omega = c / \lambda_0$, where c is the speed of light and λ_0 is the wavelength of the incident light in a vacuum. The vector $\mathbf{q}$, called the "scattering vector," is a fundamental characteristic of any scattering process (Fig. 1). In a uniform medium, in which each point in space produces a wave with the same amplitude, the sum in Eq. 1 equals zero when $q \neq 0$ and the light only propagates in the forward direction, where $q = 0$. Scattering thus only occurs from medium inhomogeneities, such as those caused by solute particles or by density fluctuations in an otherwise uniform solvent.

The intensity I of the scattered light is proportional to the square of the amplitude of the electromagnetic field, that is:

$$I = A_0 \left| \sum_k \mathbf{E}_k \exp(i\mathbf{q}\cdot\mathbf{r}_k) \right|^2 . \tag{2}$$

Here A_0 is a coefficient that depends on the geometry of light collection. Equation 2 describes mathematically the interference

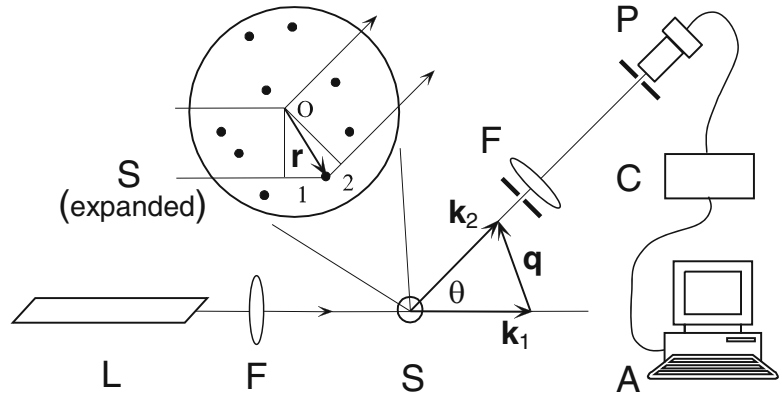

Fig. 1. Block scheme of the QLS setup. Laser (L); Focusing and collecting optics (may include optic fibers) (F); Sample cuvette (S); Photodetector (P); Correlator (C); data Analysis workstation (A). The scattering vector **q** (see expanded view of S): The path traveled by a wave scattered at the point with radius vector **r** differs from the path passing through the reference point O by two segments, 1 and 2, with lengths l_1 and l_2, respectively. The phase difference is $\Delta\varphi = k(l_1 + l_2)$, where $k = 2\pi n / \lambda_0$ is the absolute value of the wave vector and n is the refractive index of the scattering media. The segment l_1 is a projection of **r** on the wave vector $\mathbf{k}_1$ of the incident beam, i.e. $kl_1 = \mathbf{k}_1\mathbf{r}$. Similarly, $kl_2 = \mathbf{k}_2\mathbf{r}$, where $\mathbf{k}_2$ is a wave vector of the scattered light. Thus $\Delta\varphi = (\mathbf{k}_1 - \mathbf{k}_2)\mathbf{r}$. The vector $\mathbf{q} = \mathbf{k}_1 - \mathbf{k}_2$ is called the scattering vector. The absolute value of **q**, $q = 4\pi n / \lambda_0 \sin\theta / 2$, where θ is the angle of scattering.

pattern, or "speckles" produced by waves scattered by a set of scattering particles located at positions $\mathbf{r}_k$. As these particles move, the intensity varies with time around its average value, $I_0 = \sum I_k$, where $I_k = A_0 \mid \mathbf{E}_k \mid^2$ is the intensity of light scattered by the kth particle.

The intensity of scattering by an individual particle, I_k, is proportional to Δn^2, where Δn is the difference between the refractive index of the particle and that of the media. I_k also depends on particle mass and shape. Let us consider an aggregate composed of m monomers, each producing a scattered electromagnetic wave $\mathbf{E}_0$. If the size of the aggregate is small, so that each $\mathbf{q}\cdot\mathbf{r}_k$ in Eq. 2 is essentially the same, then for this aggregate $\mathbf{E}_k = m\mathbf{E}_0$. The intensity of the light scattered by the small aggregate thus is proportional to the square of its molecular weight. The quadratic dependence of scattering intensity on the mass of the scatterer is the basis for the optical determination of the molecular weight of macromolecules and for various turbidimetry and nephelometry techniques. If an aggregate is not small as compared to the light wavelength, the destructive interference of waves scattered from different points in the particle reduces the intensity of light scattering by a factor of $|\alpha|^2 < 1$, where $\alpha(\mathbf{q})$ is an averaged value of the $e^{i\mathbf{q}\cdot\mathbf{r}_k}$ for all monomers. After being averaged over all possible orientations of the particle relative to the scattering vector **q**, the factor $|\alpha|^2$, the "structure factor," is obtained. A table of expressions for the

structure factors for particles of various shapes can be found elsewhere (8). The structure factor depends on the absolute value of the scattering vector, $q = 4\pi n / \lambda_0 \times \sin(\theta/2)$ and thus defines the angular dependency of the intensity of scattered light. The measurements of this angular dependency can, therefore, be used to determine the size and shape of sufficiently large scattering particles.

In QLS, the photodetector registers the random temporal fluctuations of the intensity of the scattered light, $I(t)$. The resulting correlation function of the intensity fluctuations is computed according to Eq. 3:

$$G^{(2)}(\tau) = \langle I(t) I(t+\tau) \rangle, \tag{3}$$

in which the angular brackets denote an average over time t. One common approach to calculate $G^{(2)}(\tau)$ is to store the numbers of photons registered by the photodetector within short consecutive time intervals Δt. These photon counts represent instantaneous values of the scattered light intensity. According to Eq. 3, to obtain the correlation function $G^{(2)}(\tau)$ at $\tau = n\Delta t$, the average product of counts n intervals apart should be determined. Modern correlators simultaneously accumulate several hundred of these products without loss of information, with Δt in the nanosecond range.

The intensity of the scattered light fluctuates due to the motion of the scattering particles, in particular through their diffusion. According to Eq. 1, electromagnetic waves scattered by a pair of individual particles have, at the observation point, a phase difference $\mathbf{q}\cdot\Delta\mathbf{r}$, where $\Delta\mathbf{r}$ is the vector distance between particles. As the scattering particles move over distance $\Delta x \approx q^{-1}$, the phases for all pairs of particles change significantly and the intensity of the scattered light becomes independent of its initial value. Thus the correlation time of the intensity fluctuations, τ_c, is the time required for a particle to move a distance q^{-1}. The laws of diffusive motion stipulate that the mean square displacement of a particle with a diffusion coefficient D over time Δt is characterized by the relationship $\Delta x^2 = 2D\Delta t$. Thus for $\Delta x \approx q^{-1}$, $\tau_c \approx 1/Dq^2$. Mathematical analysis of light scattering by a solution of many small, noninteracting particles leads to the following expression for the intensity correlation function defined by Eq. 3:

$$G^{(2)}(\tau) = I_0^2 \left(1 + \gamma \left| g^{(1)}(\tau) \right|^2 \right) \tag{4}$$

Here I_0 is the average intensity of the detected light and γ is the efficiency factor, which depends on the size of the scattering volume and the angle in which scattered light is collected. The key element in Eq. 4 is the instrument-independent, normalized field correlation function $g^{(1)}(\tau)$. For a particle undergoing diffusive Brownian motion, the field correlation function is a pure

exponential, $g^{(1)}(\tau) = e^{-\tau/\tau_c}$, with the decay time $\tau_c = 1/Dq^2$, in accord with the above considerations. When many scattering particles are present,

$$g^{(1)}(\tau) = \frac{1}{I_0}\sum_k I_k e^{-D_k q^2 \tau}. \quad (5)$$

In a monodisperse system, when all scatterers are the same, Eq. 5 reduces to $g^{(1)}(\tau) = e^{-Dq^2\tau}$ allowing immediate determination of the diffusion coefficient D from the experimental data by fitting $g^{(1)}(\tau)$ with a single exponential function. For a spherical particle, the relation between its radius R_h and its diffusion coefficient D is given by the Stokes–Einstein (9) equation:

$$R_h = \frac{k_B T}{6\pi\eta D}. \quad (6)$$

Here k_B is the Boltzmann constant, T is the absolute temperature, and η is solution viscosity. For nonspherical particles, Eq. 6 defines the *apparent* hydrodynamic radius of the particle. The apparent hydrodynamic radius can be calculated numerically, and in some cases analytically, for a variety of particle shapes (10).

In polydisperse systems, i.e., where a variety of particles is present in the solution, the reconstruction of the size distribution of scattering particles from an experimentally measured correlation function is a complex mathematical problem. The difficulty stems from the fact that different distributions with similar smoothed, averaged characteristics can fit the experimental data equally well. The simplest approach to deal with this difficulty is to assume the functional form of the distribution a priori (single modal, bimodal, Gaussian, etc.). The parameters of the assumed distribution that lead to the best fit to the experimental data then can be determined. The value of this method depends on the validity of the assumed distribution. It has the potential to "confirm" any a priori assumption made, especially if excessive numbers of free parameters are used in the fitting procedure. In practice, typical QLS data allow reliable determination of no more than three independent parameters of the size distribution of the scattering particles.

The cumulant method, in contrast, is free from bias introduced by a priori assumptions. In this approach, the focus is not on the shape of the distribution but instead on its average characteristics, such as the moments of the distribution or closely related quantities called cumulants (11), which are derivatives of the logarithm of the correlation function $g^{(1)}(\tau)$ at $\tau = 0$. The first cumulant of the distribution, the initial slope of the normalized correlation function, gives the average diffusion coefficient $\bar{D}$. Indeed, using Eq. 5, it is straightforward to show that:

$$-\frac{d}{d\tau}\ln g^{(1)}(\tau)\Big|_{\tau=0} = \frac{1}{I_0}\sum_k I_k D_k q^2 \equiv \bar{D}q^2. \quad (7)$$

The second cumulant of the distribution, the dispersion $\overline{\Delta D^2}$, can be obtained from the curvature (second derivative) of the initial part of the correlation function. The typical QLS experiment allows determination of the first moment, $\bar{D}$, with better than ±1% accuracy. The second moment, i.e., the width of the distribution $\overline{\Delta D^2}$, can be determined with an accuracy of ±5–10%. The third moment, which characterizes the asymmetry of the distribution, usually can be estimated with an accuracy of only about ±100%.

A third method, the regularization approach, combines the best features of both of the previous methods. It assumes that the distribution is an arbitrary, but smooth, function and seeks a non-negative distribution producing the best fit to the experimental data. The requirement of smoothness precludes spikes in the distribution, allowing a unique solution to the minimization problem. The choice of the smoothness parameter is the most important part of the regularization method. A well-chosen value for the smoothness parameter produces stable, reproducible results in repetitive measurements of the same correlation function. If the magnitude of the smoothing is too great, the distribution, though stable, will lack details. Regularization analysis can resolve a bimodal distribution with two narrow peaks of equal intensity, if the diffusion coefficients corresponding to these peaks differ by more than a factor of ~2.5. Figure 2 illustrates how the smoothing parameter

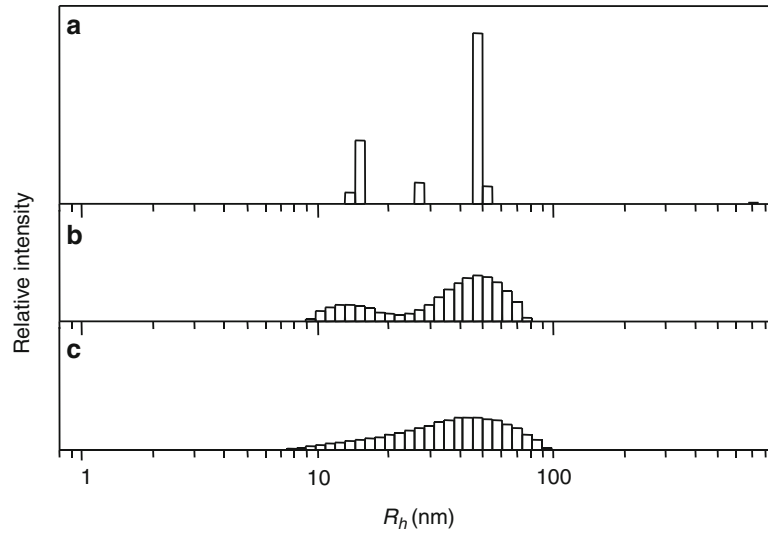

Fig. 2. Oligomer size distribution of Aβ. (**a**) A distribution computed with insufficient smoothing. Peaks positions in this distribution are not reliable, even though they provide the best fit to the experimental data. (**b**) A properly chosen regularization parameter allows observation of two populations, oligomers with hydrodynamic radii of 10–20 nm and their aggregates with average radius of ≈60 nm. This distribution is stable and does not vary significantly among measurements. The average deviation from the experimental data is only 0.5% larger than in (**a**). (**c**) An excessively smoothed distribution does not show separate oligomer and aggregate populations. This distribution is stable and also fits the experimental data well, with an average deviation only 3% more than in (**a**), but important details are not resolved.

choice can affect data interpretation. There are several regularization algorithms that differ in the specific mathematical implementation of the smoothness condition. One popular program is called CONTIN (12). We have developed and use the regularization procedure described in ref. (13). Our algorithm is also utilized in PrecisionDeconvolve software supplied with QLS instruments produced by Varian (USA) [formerly by Precision Detectors (USA)].

3. QLS Setup

A variety of QLS instruments is available commercially. Among the suppliers of QLS systems are ALV (Germany), Brookhaven Instruments (USA), Malvern Instruments (UK), and Wyatt Technology (USA). It is also possible to purchase the key elements of the QLS setup: laser, photodetector, and correlator separately and to build a custom system on an optical table using standard optical hardware. Our current QLS system uses a He–Ne laser (wavelength 633 nm and power 50 mW) from Coherent (USA) as a light source. The photodetector is an APT (avalanche photodiode) built into the PD4047 multitau correlator from Varian (USA). A 90° scattering geometry generally is used for monitoring the protein assembly.

There are several requirements that must be met to perform a successful QLS experiment. Conditioning of the incident laser beam is one important factor. The beam must produce a sufficient intensity of scattered light. If the photodetector count rate drops below 1 photocount per correlation time, the accuracy with which the correlation function can be measured decreases significantly. Conversely, an excessively intense incident beam may increase the temperature in the scattering volume. Because the diffusion coefficient is temperature-dependent, heating causes errors in its determination. To control for heating effects, especially when an accurate absolute measurement of scattering particle size is desired, one can do measurements at several intensities of the incident beam. The fluctuations in laser intensity make the factor I_0^2 in Eq. 4 dependent on delay time τ. This dependence affects the determination of $g^{(1)}(\tau)$, especially when the efficiency factor γ is small. At a given scattering angle, maximum scattering occurs in a plane perpendicular to the direction of the incident light polarization. Therefore, the incident beam should be polarized perpendicular to the plane formed by light source, sample, and photodetector. If the illuminating light is delivered via optical fiber, care should be taken to ensure that the vibrations of the fiber do no translate into significant fluctuations in the polarization of the incident beam.

To minimize the effect of stray light, the collecting optics is designed to pick up only light from a small collection volume

within the sample. The intersection of this volume and the volume illuminated by the incident beam is termed the "scattering volume." The scattering volume is an important factor in the QLS experiment. Reducing the scattering volume by focusing the incident beam, without significant loss of total scattering intensity, can be beneficial. Light from a smaller volume is coherent within a wider angle, allowing efficient collection of the scattered light from within a larger solid angle. If the light is collected within an angle wider than the coherence angle, averaging over several independently fluctuating speckles occurs. This reduces the efficiency factor γ in Eq. 4 and thereby only magnifies the effects of instability of the incident beam without improving the signal-to-noise ratio in the correlation function.

4. Large Aggregates and Intensity Spikes

As explained above, the intensity of scattering by an individual particle, I_k, is proportional the square of the molecular weight of the particle. For example, when dimer is formed it scatters twice as much as two monomers separately. When dense 1,000-particle aggregates (with a hydrodynamic radius about ten times that of a monomer) form, only 0.1%, by weight, of such aggregates produces the same scattering intensity as all the remaining monomers combined. The contribution of such an aggregate can be observed easily, which is one reason why the QLS method is well suited for detecting and studying the aggregation of particles in solution. However, these same considerations mean that even a small fraction of large impurities, for instance dust particles, can significantly affect light scattering. The easiest way to remove large impurities from solution is by filtration. Standard 0.22 μm filters are often too porous to be of use. We have found that 20 nm Anatop filters are satisfactory in most studies of protein aggregation. Centrifugation is another effective way to remove large impurities from the solution, provided that the sample is spun in the same sealed cuvette in which the QLS measurements will be done. Typical airborne dust can be pelleted in 30 min at $5{,}000 \times g$. However, "flaky" dust particles will not sediment by this procedure. A very useful, though cumbersome, method of sample purification is to utilize liquid chromatography to elute the desired fraction into a flow-through QLS cuvette (14).

During protein assembly in a closed system, the total amount of material does not change. Therefore, as the size of aggregates increases, the total particle number decreases. This often leads to a situation in which the number of aggregates, N, in the scattering volume is small. This can preclude accurate analysis of correlation

functions in QLS. Indeed, Eq. 4 for the intensity correlation function is applicable to the intensity fluctuations due to the temporal variations in the interference pattern produced by scattering particles as they move relative to each other. As Eq. 4 stipulates, $G^{(2)}(\tau) \sim I_0^2$. Equation 4 ignores intensity fluctuations caused by drifting of scattering particles into and out of the scattering volume. The relative fluctuation in the number of particles in the scattering volume is $N^{-1/2}$, the corresponding intensity fluctuations are I_0 / N, and the contribution of this effect in the intensity correlation function is therefore I_0^2/N. Thus, the relative magnitude of this contribution is proportional to $1/N$, and it may be ignored only when $N \gg 1$.

Fluctuations in the number of particles within the scattering volume can be measured using fluorescence correlation spectroscopy (FCS) (15). In FCS, the radiation is incoherent, factor γ in Eq. 4 is effectively zero, and only intensity fluctuations associated with position, orientation, or state of individual particles are measured. The FCS technique can be used to evaluate the size and concentration of particles in solution. However, in FCS, the intensity correlation function depends on the geometry of illumination and light collection and is difficult to analyze, especially in a multicomponent system.

In studies of systems in which aggregation occurs, it is important to recognize when the intensity fluctuations associated with the movement of individual particles through the scattering volume can significantly affect the analysis of the QLS data. This can be done by monitoring the scattered light intensity averaged over a relatively short time interval. In our measurements, we typically choose this time interval to be 1 s. Let us evaluate the expected "normal" QLS variations in the average intensity. The instantaneous relative amplitude of intensity fluctuations is given by factor γ in Eq. 4, and ideally can reach 100%. However, the correlation time of these fluctuations in the interference pattern is small. For example, a particle with a hydrodynamic radius of 15 nm in water at room temperature has, according to Eq. 6, a diffusion coefficient $D \approx 1.5 \times 10^{-11}$ m^2/s. For a He–Ne laser ($\lambda = 633$ nm) and a 90° scattering angle in water (the index of refraction $n = 1.33$), the scattering vector $q = 1.87 \times 10^{-7}$ m^{-1}. It is easy to estimate than that the intensity correlation time, $\tau = 1/(2Dq^2) \approx 10^{-4}$ s. For particles with smaller R_h, τ is proportionally smaller. The intensity averaged over 1 s thus includes at least 10^4 independent realizations of instant intensity each of no more than 100% in magnitude. We, therefore, expect typical average intensity fluctuations inherent for QLS to be less than 1%.

The same 1% level of fluctuations in the number of particles requires 10,000 particles ($N^{-1/2} = 0.01$) in the scattering volume. For comparison, for a 0.1 mM solution in a scattering volume of $10 \times 10 \times 10$ μm, we expect to have about 0.6×10^8 particles and

thus a practically negligible relative number of fluctuations of $\approx 10^{-4}$. However, if in the process of aggregation, 0.1% of these monomers form 1,000-monomer aggregates, there will be only about 60 of these aggregates in the scattering volume and the relative intensity fluctuations will be 13%. The correlation function for these fluctuations depends on the size and geometry of the scattering volume. Under these circumstances, accurate determination of the sizes of particles in solution becomes difficult. Further increases in the size of aggregates and decreases in their numbers may eventually result in a situation in which most of the time there are no aggregates in the scattering volume. At rare time intervals, when an aggregate is inside the scattering volume, a large spike in intensity will be observed.

Figure 3 illustrates the manifestations of the aggregation process that leads to the formation of few large aggregates. The topmost panel shows data taken soon after sample preparation on May 13. We observe scattering from oligomers of R_H mostly between 15 and 30 nm, with some contributions from small particles, including monomers or dimers. The intensity fluctuations are "normal," i.e., below 1%. After 5 days of incubation, large 100 nm aggregates are formed. The contribution from the smaller 15–30 nm oligomers is still observable, but the scattering from monomers cannot now be detected. Intensity fluctuations have increased to about 10%, indicating that the number of large aggregates in the scattering volume is now small. After 14 days of incubation, very big aggregates are formed which now are too few to be found in the scattering volume all the time. Instead, they drift in and out of the scattering volume

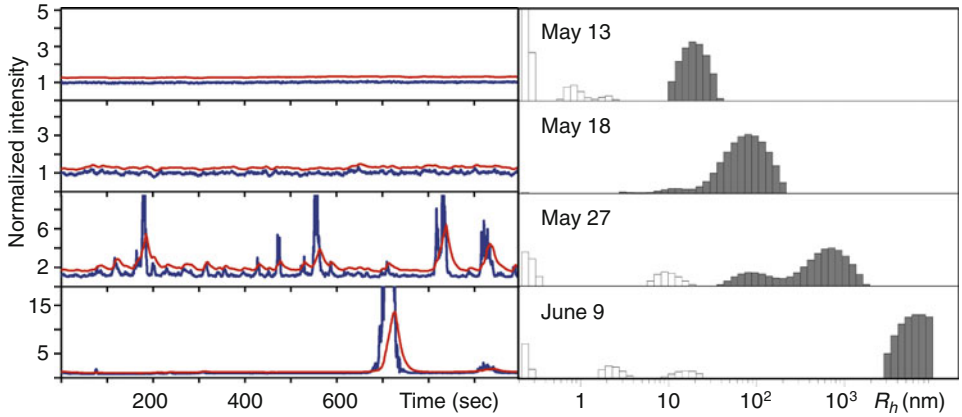

Fig. 3. Intensity spikes produced by large aggregates diffusing through a scattering volume. Normalized intensity fluctuations averaged over 1 s intervals during 1,000 s measurements (*left panels*) and the corresponding normalized size distributions (*right panels*) in an Aβ42 sample (concentration is 0.4 mM; data are from (16)). The panels show data immediately after sample preparation and then 5, 14, and 27 days later, from top to bottom. The date of measurements is shown in the distribution panels. In the *left panels*, the *blue lines* are intensity profiles and the *red lines* are intensity cutoff levels (see text). Note the changing scale in the normalized intensity and the fact that in the bottommost panel the main intensity spike is out of scale (it is actually >60 times the background intensity).

producing intensity spikes up to ten times the background scattering intensity from the sample. Finally, after about a month of incubation, very few very large aggregates are left in the solution. These aggregates produce huge intensity spikes when they occasionally enter the scattering volume.

When large aggregates are an integral part of a system and cannot be removed, or reform rapidly after filtration, "software dust filtering" can be done. This approach interrupts data accumulation during spikes in intensity caused by large particles passing through the scattering volume. Red lines in the intensity panels in Fig. 3 represent these intensity cutoff levels. When the intensity exceeds this level the data are discarded. In Fig. 3, the cutoff levels were set to be sliding average of the previous 10 s of measurements below the cutoff level. Some scattering from within intensity spikes was registered in this case to document the presence of large particles. If minimizing the effects of intensity spikes is desired, it can be beneficial to focus the laser beam to make the scattering volume as small as possible. Spikes in intensity associated with large particles in the scattering volume then become larger in intensity, but shorter in time and less frequent. This allows for better discrimination between these spikes and the regular intensity fluctuations.

Our in-house acquisition software can store correlator output every 0.1 s and later "replay" these measurements. This allows an effective exclusion of intensity spikes from the data analysis, leading to improvement in the quality of measurement of oligomer populations. Additionally, it is possible to obtain statistical information regarding spike frequency and intensity. This provides the means to quantify and to compare the process of formation of very large aggregates among different samples (17). It also is possible to determine the correlation function within the spikes. However, the interpretation of such correlation functions is very much dependent on the model adopted for the structure and dynamics of the aggregates.

5. QLS Monitoring of Fibril Assembly

The hydrodynamic radius of a small thin fibril with length L and diameter d, where $L >> d$ is approximately $R_h = L / \ln(L / 2d)$ (10). As fibrils grow in length, the diffusion of the fibril over distances of the order of q^{-1} becomes dependent on fibril orientation. The intensity of the scattering by a large fibril also depends on its orientation. As a result, the orientational diffusion of fibrils with length $L \geq q^{-1}$ ($q^{-1} \sim 100$ nm) plays an important role in QLS and produces a complex nonexponential correlation function even in monodisperse systems. These effects usually are subsumed into the definition of the apparent hydrodynamic radius of the fibril. In this

definition, the inverse average relaxation time of the multiexponential correlation function given by the left side of Eq. 7 is used to calculate the apparent diffusion coefficient, $\bar{D}$, which is then used in Eq. 6 to calculate R_h.

When the length of the fibril becomes comparable to the persistence length l_p (18), the effects of fibril flexibility must be taken into account. Flexibility adds even more complexity to the anisotropic diffusion and orientational dynamics of a fibril. Effects of flexibility on the correlation function have been discussed in detail by Maeda and Fujume (19). For the same length, a flexible fibril will have a smaller R_h than will a rigid one. Fibrils which are much longer than the persistence length form coils with apparent hydrodynamic radii of $R_h = 0.94\sqrt{l_p L}$. Fortunately, amyloid fibrils are rigid, thus their flexibility typically is not a factor in QLS experiments.

The most serious factor affecting the interpretation of QLS data on growing fibrils is fibril–fibril interaction. When the distance between fibrils is less than the fibril length (the "semidilute regime") fibrils cannot move perpendicular to their long axes because of caging by other fibrils. They only diffuse along their axes (20). The average distance between fibrils is $\sim N^{-1/3}$, where N is the number of fibrils in a unit volume, $N \approx \varphi / Ld^2$, and ϕ is the volume fraction occupied by fibrils. According to this estimate, $L \geq N^{-1/3}$ when $L \geq d/\sqrt{\varphi}$. Thus, regardless of the concentration, sufficiently long rigid fibrils always enter the semidilute regime. QLS on semidilute solutions of rods has been discussed by Zero and Pecora (21) and reviewed by Russo (22). Qualitatively, fibril–fibril interaction in a semidilute solution dramatically slows down diffusion of fibrils, and if unaccounted for, leads to gross overestimation of fibril length.

6. Amyloid β-Protein Self-Assembly

Amyloid β-protein (Aβ) fibrillogenesis plays a seminal role in the pathogenesis of Alzheimer's disease (4). QLS can be used to monitor quantitatively the temporal evolution of the fibril length distribution in solutions of synthetic Aβ, allowing determination of the rate constants for fibril nucleation and elongation (23, 24). Knowledge of these parameters allows modeling of the fibrillogenesis process and evaluation of the effect of chemical agents or solution condition on the process. Aβ fibrils have diameters $d \approx 6$–10 nm. At Aβ concentration $C = 0.1$ mM, Aβ fibrils occupy a volume fraction $\phi = 2 \times 10^{-3}$, and the semidilute regime in this solution occurs when fibrils are longer than 150 nm. This length is close to the estimated persistence length of Aβ fibrils (25) and is comparable to $q^{-1} \sim 100$ nm. These estimates imply that the

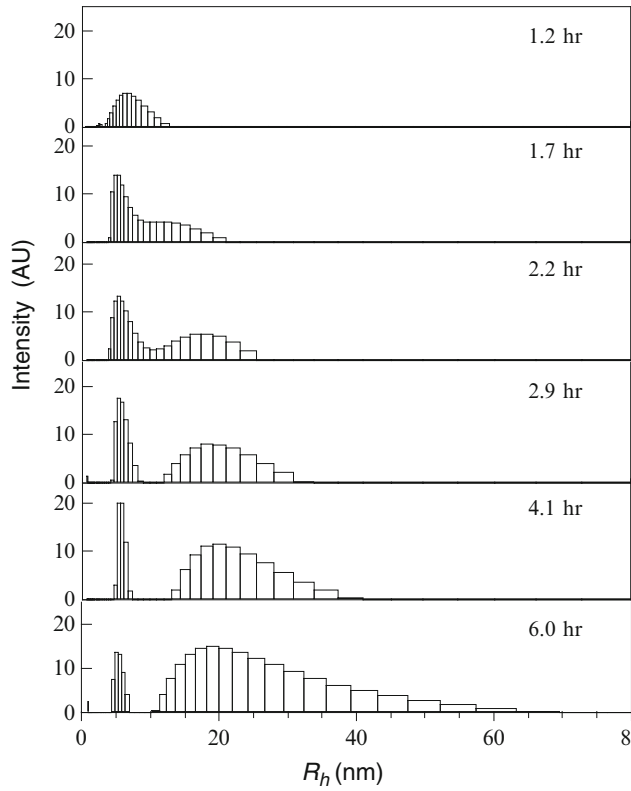

Fig. 4. Temporal evolution of the size distribution of the scattering particles in 0.25 mM solution of Aβ(1-40) in 0.1 N HCl. A freshly prepared and filtered sample contains particles with $R_h \sim 7$ nm. These particles were identified as micelles consisting of ~30 Aβ monomers (23, 26). As time progresses, a second distribution of larger particles emerges. These are Aβ fibrils that grow in size over time. Simultaneously, new fibrils are nucleated from micelles so that shorter fibrils are always present. Adapted from (27).

quantitative analysis of fibril assembly by QLS is most appropriate at the critical early stages of fibril assembly, when fibril length does not exceed 100–150 nm. At later stages, when solutions contain longer fibrils, structural information still can be obtained, but it is more qualitative in nature. Figure 4 shows an example of QLS monitoring of Aβ fibril nucleation and growth.

Hydrodynamic radii of fibrils can be converted into fibril lengths, and thus the elongation rate of the fibril can be determined. This is an extremely powerful capability. It enables quantitative study of fibril elongation reactions under different conditions, including alterations in peptide concentration, temperature, pH, ionic strength, or addition of cosolvents, thus providing insight into physical–chemical mechanisms underlying fibrillogenesis. Quantitative study of fibril growth also allows evaluation of the effects of chemical agents and changes in Aβ sequence that may facilitate or inhibit fibrillogenesis. As an example, Fig. 5 illustrates an experiment performed by dissolving HPLC-purified Aβ(1-40),

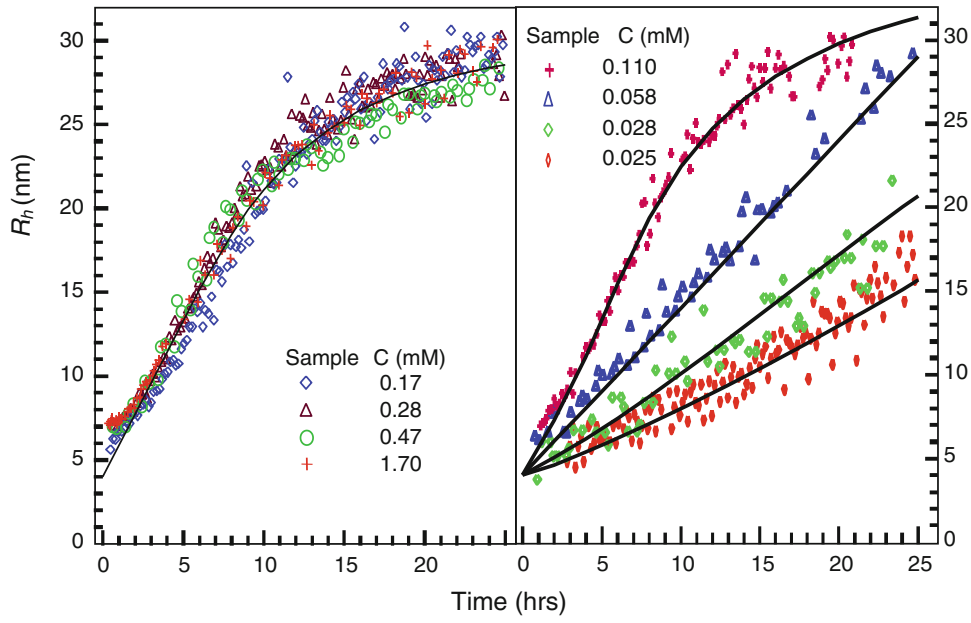

Fig. 5. Concentration dependence of Aβ fibrillogenesis. The *left panel* shows the temporal evolution of the average hydrodynamic radius R_h of scattering particles in solution with Aβ concentration above the critical micellar concentration (CMC; ~0.1 mM). An initial size of R_h ~ 7 nm observed at higher concentrations is due to the presence of micelles shown in Fig. 4. The *right panel* shows the evolution of average fibril size at concentrations at and below the CMC. *Solid lines* are eye guides. Adapted from (23).

at concentrations ranging from 25 μM to 1.7 mM, in 0.1 N HCl. For each concentration, ~200 μl of sample were placed in a 5 mm diameter glass test tube and then centrifuged at 5,000×*g* for 30 min to pellet dust particles and large aggregates. The tube then was placed into the QLS spectrometer and the intensity and correlation function of the scattered light measured periodically over the next 20–50 h. During the monitoring period, the sample remained at ~22°C. Figure 5 demonstrates that when Aβ concentration is above the critical concentration of approximately 0.1 mM, the temporal evolution of fibril is independent of concentration, indicating a constant elongation rate and a nucleation rate proportional to the total Aβ concentration. Below 0.1 mM, the elongation rate drops. The nucleation rate drops as well, resulting in fewer fibrils with larger average lengths (data not shown). These findings allowed us to conclude that, in these experiments, Aβ monomers form micelles at monomer concentration exceeding the CMC (23). As a result, the fibril elongation rate (~9 monomers/h) remains constant above the CMC. Moreover, these micelles serve as fibril nucleation centers (with a micelle-to-fibril conversion rate of 0.11/day). Thus the nucleation rate is proportional to the concentration of Aβ in excess of the CMC, and the rate drops dramatically when the total Aβ concentration is below the CMC.

Examples above from studies of Aβ fibrillogenesis illustrate the power of the quantitative capabilities of QLS to elucidate molecular mechanisms of fibrillogenesis reactions and guide development of fibrillogenesis inhibitors.

Acknowledgments

This work was supported by NIH grant AG027818 and the Jim Easton Consortium for Alzheimer's Drug Discovery and Biomarkers at UCLA.

References

1. Berne, B. J. and Pecora, R. (2000) Dynamic Light Scattering with Applications to Chemistry, Biology, and Physics, Dover.
2. Schmitz, K. S. (1990) An Introduction to Dynamic Light Scattering by Macromolecules. Academic Press, Boston.
3. Schärtl,W. (2007) Light Scattering from Polymer Solutions and Nanoparticle Dispersions. Springer, Berlin.
4. Herczenik, E. and Gebbink, F. B. G. (2008) FASEB J. 22: 2115–2133.
5. Sipe, J. D., Benson, M. D., Buxbaum, J. N., Ikeda, S.-I., Merlini, G., Saraiva, M. J. M., and Westermark, P. (2010) Amyloid 17: 101–104.
6. Lomakin, A., Benedek, G. B., and Teplow, D. B. (1999) Meth. Enzymol 309: 429–459.
7. Teplow, D. B., Lomakin, A., Benedek, G. B., Kirschner, D. A., and Walsh, D. M. (1997) in "Alzheimer's Disease: Biology, Diagnosis and Therapeutics", edited by K. Iqbal, B. Winblad, T. Nishimura, M. Takeda and H.M. Wisniewski) p. 313–321 John Wiley, New York.
8. Kerker, M. (1969) The Scattering of Light and other Electromagnetic Radiation. Academic Press, New York.
9. Einsten, A. (1905) Annalen der Physik und Chemie 17: 549–560.
10. de la Torre, J. G., and Bloomfield V. A. (1981) Quarterly Rev. Biophys. 14: 81–139.
11. Koppel, D. E. (1972) J. Chem. Phys. 57: 4814–4820.
12. Provencher, S. W. (1982) Comput. Phys. Commun. 27: 213–227.
13. Braginskaya, T. G., Dobitchin, P. D., Ivanova, M. A., Klyubin, V. V., Lomakin, A., Noskin, V. A., Shmelev G. E. and Tolpina, S. P. (1983) Physica Scripta 28: 73–79.
14. Walsh, D. M., Lomakin, A., Benedek, G. B., Condron, M. M., and Teplow, D. B. (1997) J. Biol. Chem. 272: 22364–22372.
15. Rigler, R., Elson, E. S. (Eds.) (2001) Fluorescence Correlation Spectroscopy, Theory and Applications, Springer, Berlin.
16. Maiti, P., Lomakin, A., Benedek, G. B., Bitan, G. (2010) Journal of Neurochemistry, 113: 1252–1262
17. Li, H., Monien, B. H., Lomakin, A., Zemel, R., Fradinger, E. A., Tan, M., Spring, S. M., Urbanc, B., Xie, C.-W., Benedek, G. B., Bitan, G. (2010) Biochemistry, 49: 6358–6364
18. Kratky, O. and Porod, G. (1949) Rec. Trav. Chim. 68: 1106–1122.
19. Maeda, T. and Fujume, S. (1984) Macromolecules 17: 1157–1167; Macromolecules 17: 2381–2391.
20. Doi, M. and Edwards, S. F. (1978) J. Chem. Soc. Faraday II 74: 1789–1802.
21. Zero, K. M. and Pecora, R. (1982) Macromolecules 15: 87–93.
22. Russo, P. S. (1993) in "Dynamic Light Scattering" (W. Brown, ed.), p. 512, Claredon Press, Oxford.
23. Lomakin, A., Chung, D. S., Benedek, G. B., Kirschner, D. A. and Teplow, D. B. (1996) Proc. Natl. Acad. Sci. USA 93: 1125–1129.
24. Lomakin, A., Teplow, D. B., Kirschner, D. A. and Benedek, G. B. (1997) Proc. Natl. Acad. Sci. USA 94: 7942–7947 .
25. Shen, C. L. and Murphy, R. M. (1995) Biophysical J. 69: 640–651.
26. Yong, W., Lomakin, A., Kirkitadze, M. D., Teplow, D. B., Chen, S.-H., and Benedek, G. B. (2002) Proc. Natl. Acad. Sci. USA 99: 150–154.
27. Kusumoto, Y., Lomakin, A., Teplow, D. B., and Benedek, G. B. (1998) Proc. Natl. Acad. Sci. USA 95: 12277–12282.